Journal of Applied Polymer Science

Improved dielectric performance of polypropylene/multiwalled carbon nanotube nanocomposites by solid-phase orientation

Xiang Lin,[1] Jie-Wei Tian,[1] Peng-Hao Hu,[1] Rohan Ambardekar,[2] Glen Thompson,[2] Zhi-Min Dang,[1] Phil Coates[2]

[1]Department of Polymer Science and Engineering, School of Chemistry and Biological Engineering, University of Science and Technology Beijing, Beijing 100083, China

[2]Interdisciplinary Research Centre (IRC) in Polymer Engineering, School of Engineering, Design, and Technology, University of Bradford, Bradford BD7 1DP, West Yorkshire, United Kingdom

Correspondence to: P.-H. Hu (E-mail: huph@ustb.edu.cn)

ABSTRACT: By means of a die-drawing technique in the rubbery state, the effect of the orientation of the microstructure on the dielectric properties of polypropylene (PP)/multiwalled carbon nanotube (MWCNT) nanocomposites was examined in this study. The viscoelastic behavior of the PP/MWCNT nanocomposites with MWCNT weight loadings ranging from 0.25 to 5 wt % and the dielectric performance of the stretched PP/MWCNT nanocomposites at different drawing speeds and drawing ratios were studied to obtain insight into the influences of the dispersion and orientation state of the MWCNTs and matrix molecular chains. A viscosity decrease (ca. 30%) of the PP/MWCNT-0.25 wt % (weight loading) melt was obviously due to the free volume effect. Differential scanning calorimetry (DSC) and wide-angle X-ray diffraction were adopted to detect the orientation structure and the variation of crystal morphology of the PP/MWCNTs. Melting plateau regions, which indicated the mixed crystallization morphology for the stretched samples, were found in the DSC patterns instead of a single-peak for the unstretched samples. We found that the uniaxial stretching process broke the conductive MWCNT networks and consequently increased the orientation of MWCNTs and molecular chains along the tensile force direction; this led to an improvement in the dielectric performance.
 J. Appl. Polym. Sci. **2016**, *133*, 42893.

KEYWORDS: composites; dielectric properties; viscosity and viscoelasticity

Received 15 June 2015; accepted 27 August 2015
DOI: 10.1002/app.42893

INTRODUCTION

The introduction of a small loading of conductive or semiconductive nanoparticles into the polymer matrix near the percolation threshold can result in a significant increase in the dielectric constant (ε) without losses in the flexibility and mechanical strength.[1–4] Most of these nanocomposites are used to develop novel applications in wave absorption or heat–electric transition,[5] but their high dielectric loss (tan δ) still confines applications in other fields. This challenge always relies on the reduction of tan δ through the design of the internal microstructure. The development of a method for preparing composites with high ε and low tan δ is a topic of great interest. In this respect, improved dielectric performance in the nanocomposites can be obtained through the artificial modulation of the internal microstructure, such as the improvement in the dispersion state of the nanoparticles, to enhance the orientation degree of the molecular chains and nanofibers and the interfacial morphology between the matrix and additives. Two routines are usually adopted for achieving this:

1. The first is the modification of the polymeric chains and nanoparticles or the improvement of the interfacial morphology between the polymeric matrix and nanoadditives. This induces better interfacial polarization or a valuable crystalline phase.[2,6–10]
2. The second method focuses on the optimization of the processing technique, the promotion of the reconstruction of the packing morphology of molecular chains, and the arrangement of additive nanoparticles.[11,12]

Multiwalled carbon nanotubes (MWCNTs)/single-walled carbon nanotubes are treated as promising candidates for achieving or enhancing functional properties by through composition with the polymeric matrix because of the high aspect ratio and low aspect weight; they present excellent electrical, mechanical, and dielectric properties.[13,14] As a cost-effective product, MWCNTs are mostly used in the practical industry for mass production. MWCNT/polymer nanocomposites with high ε values and good electromechanical properties are attracting more and more

attention.[12,15] A significant improvement in the dielectric performance of polypropylene (PP)/MWCNT nanocomposites (high ε and low tan δ values) was obtained by the foaming of the polymeric matrix because of the regular carbon nanotube (CNT) alignment around the foaming cell.[16] The growing cell during foaming promotes the displacing and rotating behaviors and leads to the transition of isotropic to regular distribution of MWCNTs.

Finding methods for obtaining a good dispersibility[17] and regular alignment of MWCNTs[11] within a highly viscous polymer matrix melt is the other biggest challenge at present. For example, the electrical conductivity was the most considered property of these polymer/conductive particle composites. A higher percolation threshold value was observed for composites prepared from melt mixing than for those prepared from a solvent solution.[18] The size of the aggregations or clusters and the random networks always largely affects the expected performance.[19] The uniform dispersion of additive reinforcements in the polymer matrix and the desirable interfacial adhesion are key parameters for creating high-performance composites. In addition, the crystal-phase transition should be emphasized simultaneously in the enhancement of dielectric properties.[7,20]

Meanwhile, a regular alignment of carbon tubes, treated as crystal nuclei, is also helpful for improving the crystallization phase.[21] A clear β-crystal phase of poly(vinylidene fluoride) was observed at high nanoadditive contents,[22] and this was good for enhancing ε. The aggregated clusters, however, were important for promoting the conductive networks within the matrix because of the high aspect ratio of MWCNTs; this induced the typical insulation–conduction transition. Through the control of the percolated network structure of functionalized graphene, improved alternating-current conductivity and dielectric properties were obtained for poly(lactic acid) nanocomposites.[23] Similarly, significant decreases in the ε and conductivity of poly(vinylidene fluoride)/MWCNT nanocomposites were observed when a tensile strain was applied at room temperature because of the damage to CNT clusters or aggregations and the microstructural shift, especially at high loadings of MWCNTs.[24]

The orientation of conductive CNTs within the polymer matrix was found to be critical in improving the functional performance. The development of a method to artificially control the alignment of the CNTs in host polymers has also attracted great interest. The electrospinning technology is a simple and efficient method for obtaining a highly oriented microstructure in CNTs; this has been well reported by many laboratories.[25–27] When this requirement is proposed for practical industry, however, mass production could be the biggest challenge for preparing nanocomposites.

In this study, PP/MWCNT nanocomposites with a highly oriented microstructure were prepared by uniaxial die drawing, which was performed in the rubbery state at about 10–20°C below the melting temperature (T_m) of PP. The rheological behavior and dielectric properties of the PP/MWCNT nanocomposites were studied through melt compounding to detect the dispersion or distribution state of the MWCNTs. The effects of the crystallization morphology and alignment of the molecular chains and MWCNTs were mainly considered as the factors affecting the dielectric performance through differential scanning calorimetry (DSC), X-ray diffraction (XRD), and dielectric characterizations. We found that the die-drawing process was effective for improving the dielectric performance and decreasing ε and was also much more effective for decreasing tan δ.

EXPERIMENTAL

Materials

The polymer matrix used in this study was a commercial PP (WB 140HMS, Borealis Co.). It presented a mass density of about 0.905 g/cm^3 and a melt flow index of about 1.2 g/10 min. The MWCNTs were purchased from a domestic company (HengQiu, China). These MWCNTs presented an internal diameter of about 5–15 nm, an outer diameter above about 50 nm, a length of about 10–20 μm, a specific surface area of about 40 m^2/g, and a mass density of about 2.1 g/cm^3. A coupling agent of organic titanate was used to improve the compatibility between the PP matrix and MWCNTs during the melt-compounding process. PP/MWCNT nanocomposites with mass contents of MWCNTs of about 0.25, 0.80, 2.0, and 5.0 wt % were prepared with a batching mixer from PolyLab (Haake, Germany) at 180°C and with a rotor speed of 60 rpm. Then, these PP/MWCNTs were hot-compressed for further experimental analysis.

Apparatus

Rotational Rheometer. The rheological properties of the PP/MWCNT melts were measured with advanced rotational rheometry (MCR 501, Anton-Paar GmbH, Austria) in oscillatory mode with a frequency range of 0.1–100 rad/s at 180°C. The oscillation shear was controlled with a 1.0% strain deformation. All of the measurements were done in air environment with a parallel-plate fixture with a diameter equal to 25 mm and a constant 1-mm gap. Circular samples with a 2.0-mm thickness (d) and a 25-mm diameter were hot-compression-molded. The complex viscosity and damping factors were obtained as indices of the rheological properties.

DSC. Calorimetric measurements were performed with a Shimadzu DSC-60 instrument (Japan) under a flowing nitrogen atmosphere. Each sample was sealed in a standard aluminum pan. All of the measurements were performed at a heating rate of 10°C/min from 80 to 200°C. The tensile-strain effect on the crystalline phase transition was detected during the first heating process.

Impedance Analyzer. The dielectric properties of MgO/low-density polyethylene nanocomposites were measured with an impedance analyzer system (Agilent 4294A). Plaques, about 1.0 cm^2 in surface area, onto which silver paste was painted as electrodes, were tested under room temperature. The typical alternating-current applied voltage was 1 V, and the frequency ranged from 10^2 to 10^7 Hz. ε and tan δ were emphasized to estimate their dielectric and energy storage properties.

XRD. The investigation of the crystal morphology difference between the die-drawn samples and the unstretched samples was conducted by XRD (wavelength = 1.5406 Å, Rigaku D_{MAX}-RB 12 kW, Japan) at room temperature. The measured angle

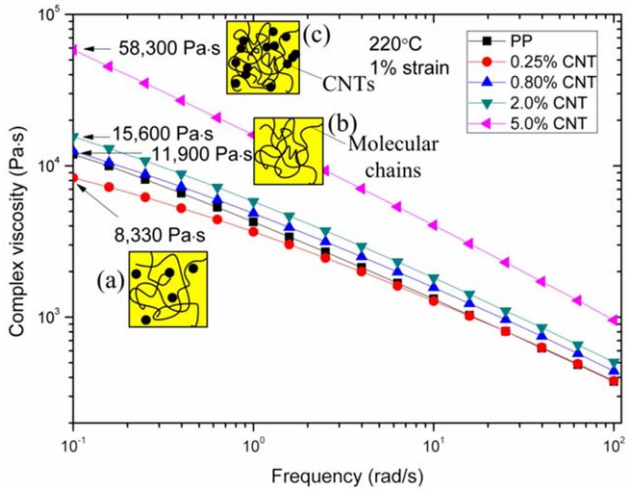

Figure 1. Complex viscosity of the PP/MWCNT nanocomposites with various MWCNT loadings. [Color figure can be viewed in the online issue, which is available at wileyonlinelibrary.com.]

ranged from 5 to 50° (i.e., $2\theta = 10–100°$) with a step width of 0.02°. To consider the orientation effect, we performed further wide-angle X-ray diffraction (WAXD) measurements for the same samples.

Scanning Electron Microscopy (SEM). The dispersion state of the MWCNTs within the PP matrix was qualitatively investigated with a scanning electron microscope (SU8010, Hitachi, Japan). The cross-sectional surface along the drawing direction was adopted for this measurement. The samples were fractured within liquid nitrogen (N_2) and a conductive coating (with Pt) was performed for the investigated surface.

RESULTS AND DISCUSSION

Rheological Behavior

The viscoelastic behavior of the PP/MWCNT melts were preferentially studied to gain fundamental insight into the optimization techniques during the processing step and to consider the effects of nanoparticles on the rheological properties. The distribution and dispersion states of the MWCNTs were found to be critical to the complex viscosity, as shown in Figure 1. Compared with the neat PP melt, a significant viscosity reduction of the PP/MWCNT-0.25 wt % melt was observed at low shear frequency. The complex viscosity decreased from 11,900 to 8330 Pa s with a percentage decrease of about 30% at a low frequency of 0.1 rad/s. Above 0.25 wt %, however, the viscosity increased abruptly with the MWCNT additive content. A viscosity percentage increase of about 390% of the PP/MWCNT-5 wt % was observed compared with the pure sample. Decreases or increases in the chains entanglement with different MWCNTs were probably responsible for these interesting results. With 0.25 wt % MWCNT addition, a better dispersion state of MWCNTs was obtained compared to that with a higher concentration. Around these MWCNT particles, the free volume increased because of the incompatibility and acted in a lubricant role during the molecular chain flowing [Figure 1(a)]. When it comes to a higher particle concentration, however, the aggregation of the nanoparticles was allowed to connect together, and this largely blocked the chain movement and led to a more serious entanglement. The formed network of particle–particle clusters performed as obstacles during the dynamic movements of the segments or macrochains during the small-oscillation shear measurements. Meanwhile, parts of the molecular chains were adsorbed onto the particle surface; this promoted new networks and decreased the dynamic activity of the molecular chains [Figure 1(c)]. The dispersion state of the MWCNTs within the PP matrix is shown in Figure 2, in which the aggregations of the MWCNTs are clearly shown. With a low content loading, several big aggregation units were individually unconnected and dispersed randomly.

Similarly, Jain *et al.*[28] and Merkel *et al.*[29] also suggested that the importance of the free volume and interaction between the nanofiller and molecular chains could not be neglected for the viscosity variation behavior. The increase in the free volume decreased dramatically the internal friction resistance among the molecular chains and led to the apparent decrease in the viscosity of the nanocomposite melts. It seemed that the generally discussed percolation threshold behavior of the nanoparticles could still be found for the viscosity variation. However, Kim *et al.*[30] pointed out that the percolation threshold was largely determined by a series of intrinsic and external factors, including the aspect ratio of the CNTs, processing conditions, polymer matrix, and additives. The effects of the aggregation on the rheological and functional properties comprise a critically complicated topic in the consideration of the waviness and three-dimensional entanglement of CNTs.

Damping factors, reflecting the viscoelasticity of the polymer melt, were also considered, as shown in Figure 3. We found that the composites with 0.25 and 5.0 wt % MWCNTs showed the maximum and a minimum damping factors, respectively, within the tested frequency range; this indicated a viscous dominant and an elastic dominant behavior, respectively. Above 0.25 wt %, the damping factor decreased with increasing MWCNT concentration. This was because apart from the sample with 0.25 wt % MWCNTs, the elastic modulus (G') increased much more with increasing nanoparticle amount than the viscous modulus (G''). The elastic behavior was much more dominant with increasing nanoparticle content because of the formation of new networks (as shown in Figure 2). In addition, the MWCNT component, which presented a much higher G', also enhanced the elastic performance of the PP/MWCNT composites when the effective composite was obtained, as presented in eq. (1):

$$G_c = G_1\varphi_1 + G_2\varphi_2 \quad (1)$$

where G_c is the modulus of the composite and G_1 and φ_1 and G_2 and φ_2 are the moduli and volume fractions of components 1 and 2, respectively. However, the decrease in the viscosity was helpful for the extrusion or injection process, increasing the melt's flowability and decreasing the swelling behavior.

Structural Investigation with DSC and XRD

The uniaxial die-drawing process was performed with an apparatus in the Polymer IRC Laboratory at the University of Bradford (United Kingdom), as shown in Figure 4. We confirmed that the best temperature for heating the billet was 10–20°C

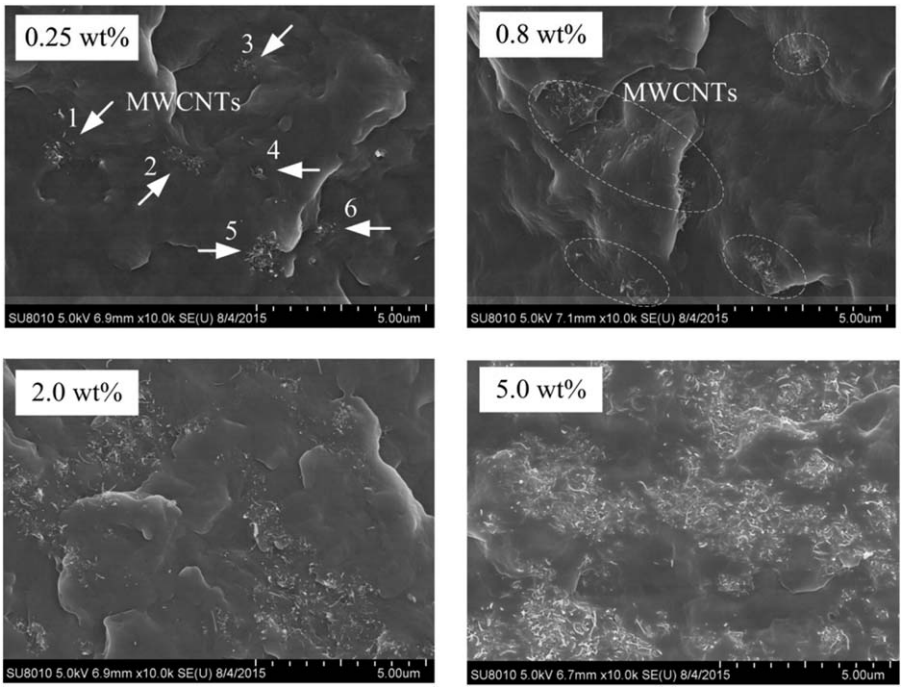

Figure 2. SEM observations of the MWCNT dispersion state at different loadings.

below its T_m.[31] In this rubbery state, the solid phase of the PP matrix was extremely stretched. In these experiments, the isotropic PP/MWCNT samples were heated to about 140°C for 5 min by hot air and with a heated die. The *d* value of the drawing product was controlled by a pair of steel plaques with a certain *d*. The solid billet was then stretched under a controlled drawing speed (*v*). In this study, steel plaques with *d*s of 0.50 and 0.25 mm were adopted to obtain drawing ratios (λs)

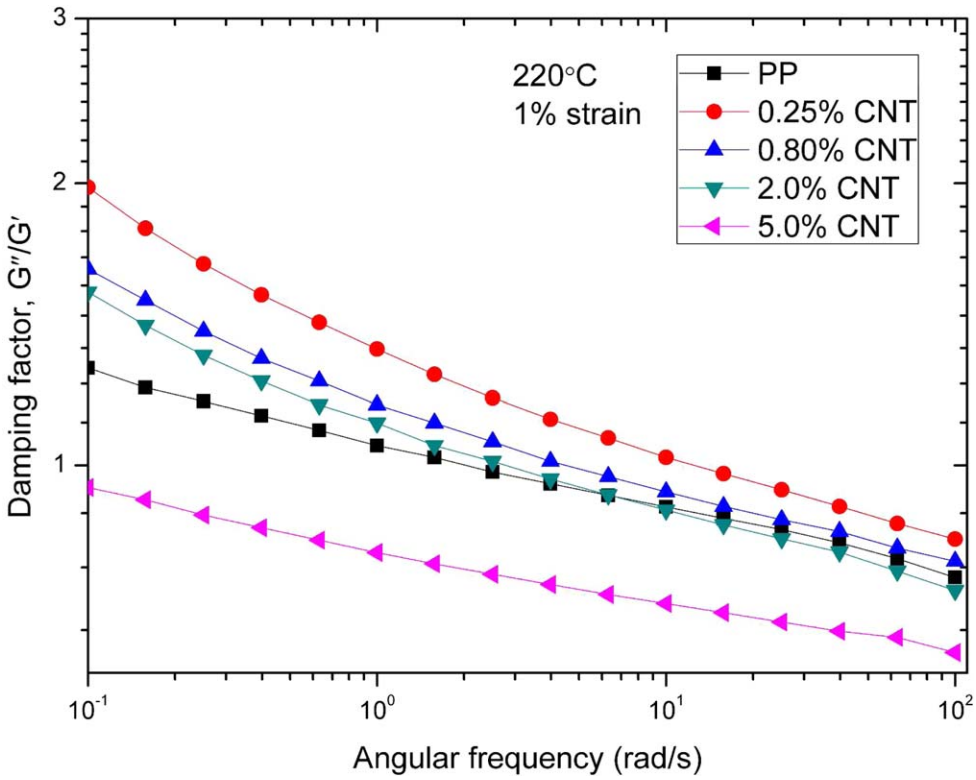

Figure 3. Damping behavior of the PP/MWCNT nanocomposites with various MWCNT loadings. [Color figure can be viewed in the online issue, which is available at wileyonlinelibrary.com.]

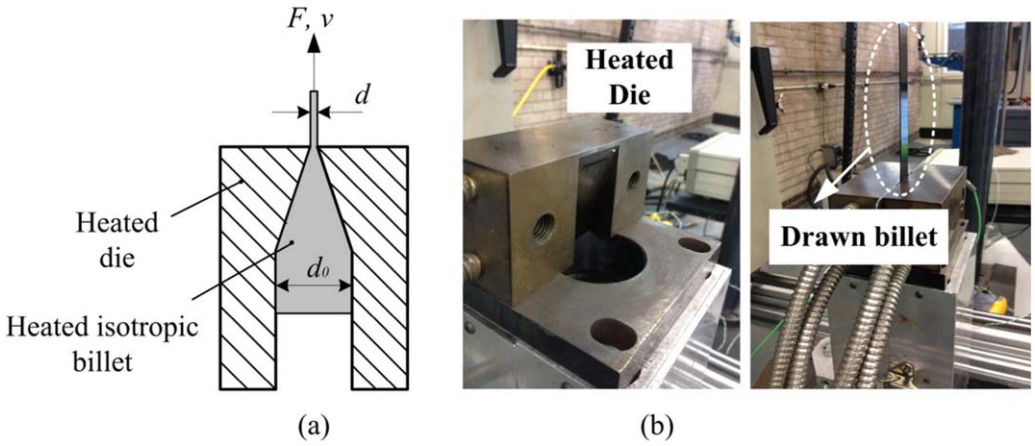

Figure 4. Schematics of the (a) die-drawing and (b) experimental apparatus. The billet was drawn under a force F and a speed v. [Color figure can be viewed in the online issue, which is available at wileyonlinelibrary.com.]

of 4.5 and 10, respectively. The drawing processes were performed at 100 and 200 mm/s to consider the effect of v on the solid-phase orientation.

λ, defined by the original thickness (d_0) divided by final d, was taken into account as the factor representing the orientation degree induced by this die-drawing process, as depicted in eq.

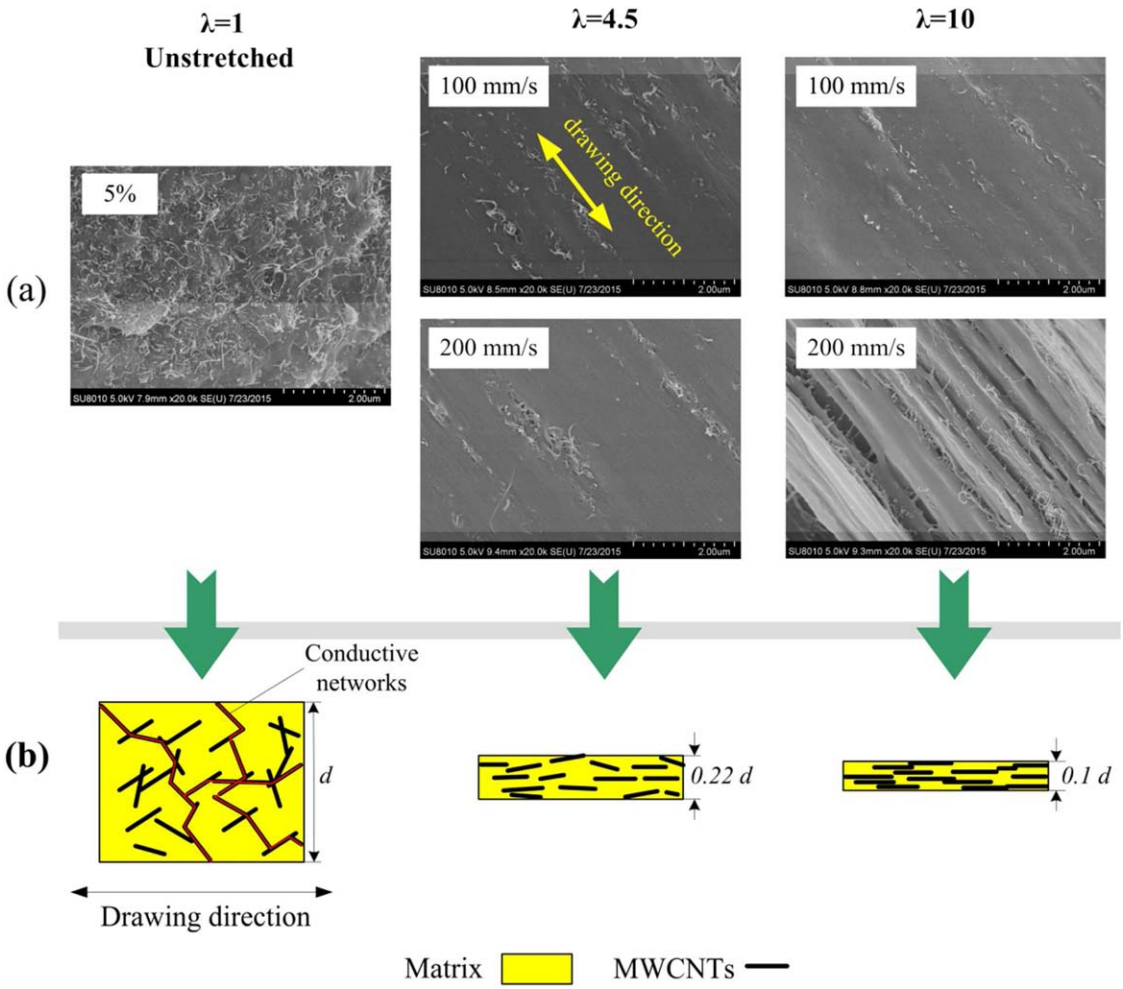

Figure 5. Comparison of the dispersion state of the MWCNTs at different λs: (a) SEM observations of the morphology of the billets before and after solid-phase orientation at different vs and λs (samples with a 5 wt % MWCNT addition were adopted) and (b) schematics of the conductive networks of the MWCNTs in the PP matrix. [Color figure can be viewed in the online issue, which is available at wileyonlinelibrary.com.]

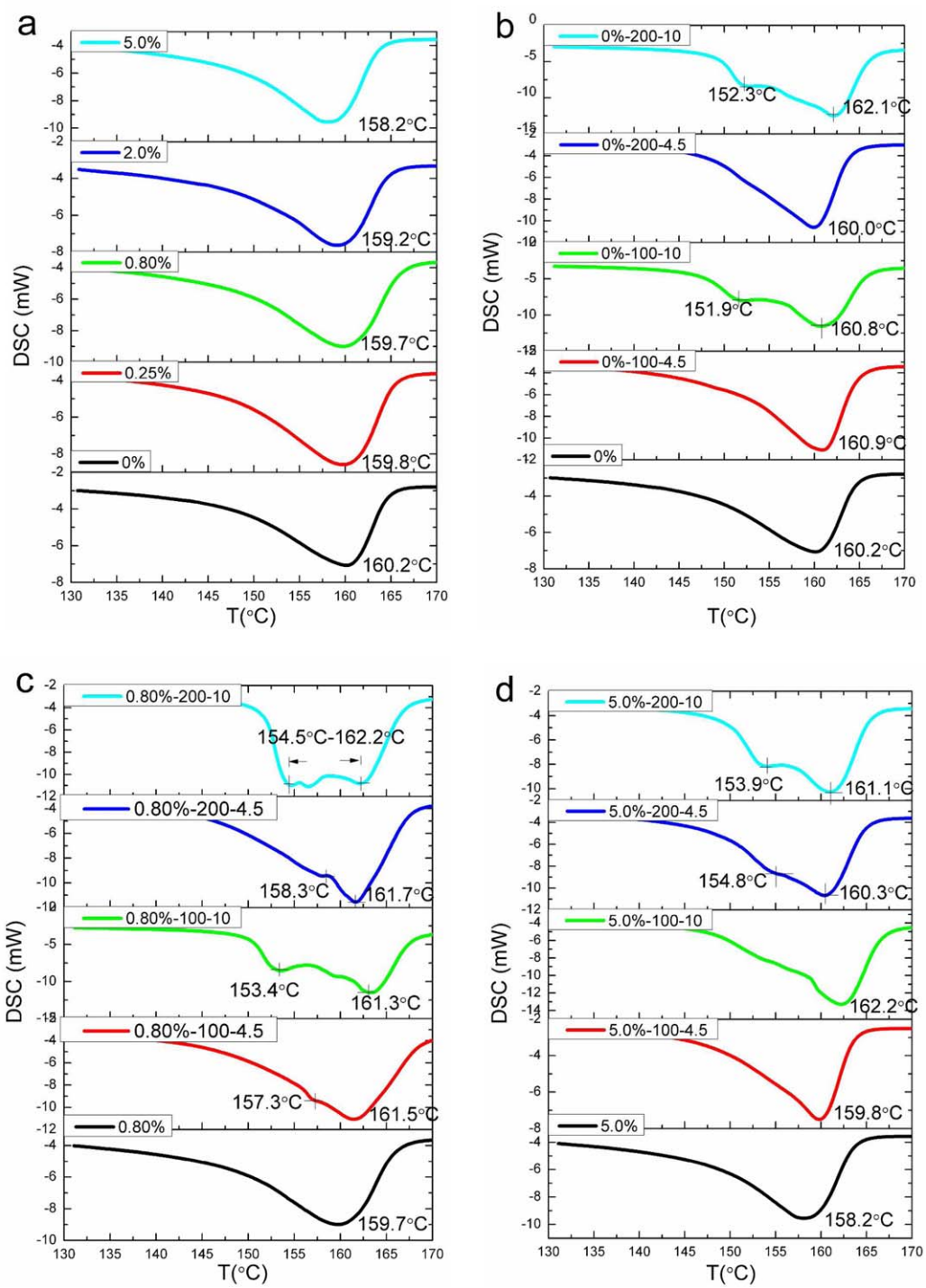

Figure 6. DSC patterns of the PP and PP/MWCNT nanocomposites with (a) different MWCNT contents and (b–d) different λs and speeds (T = temperature). [Color figure can be viewed in the online issue, which is available at wileyonlinelibrary.com.]

(2). This oriented effect was then detected by SEM observation, as shown in Figure 5. The aggregated MWCNTs were partly separated and rearranged along the drawing direction. A fibrous structure was even shown for the samples that were stretched at 200 mm/min and $\lambda = 10$. We supposed that the aggregated MWCNT clusters were originally surrounded by PP molecular chains, and then, extensional stress was applied indirectly on these clusters during the die-drawing process. This was helpful for promoting the dispersion of the aggregated MWCNTs, as shown in Figure 5(a):

$$\lambda = \frac{d_0}{d} \tag{2}$$

The crystallization morphology of the PP matrix could be significantly changed because this highly stretching process was performed in the rubbery state, in which the uniaxial

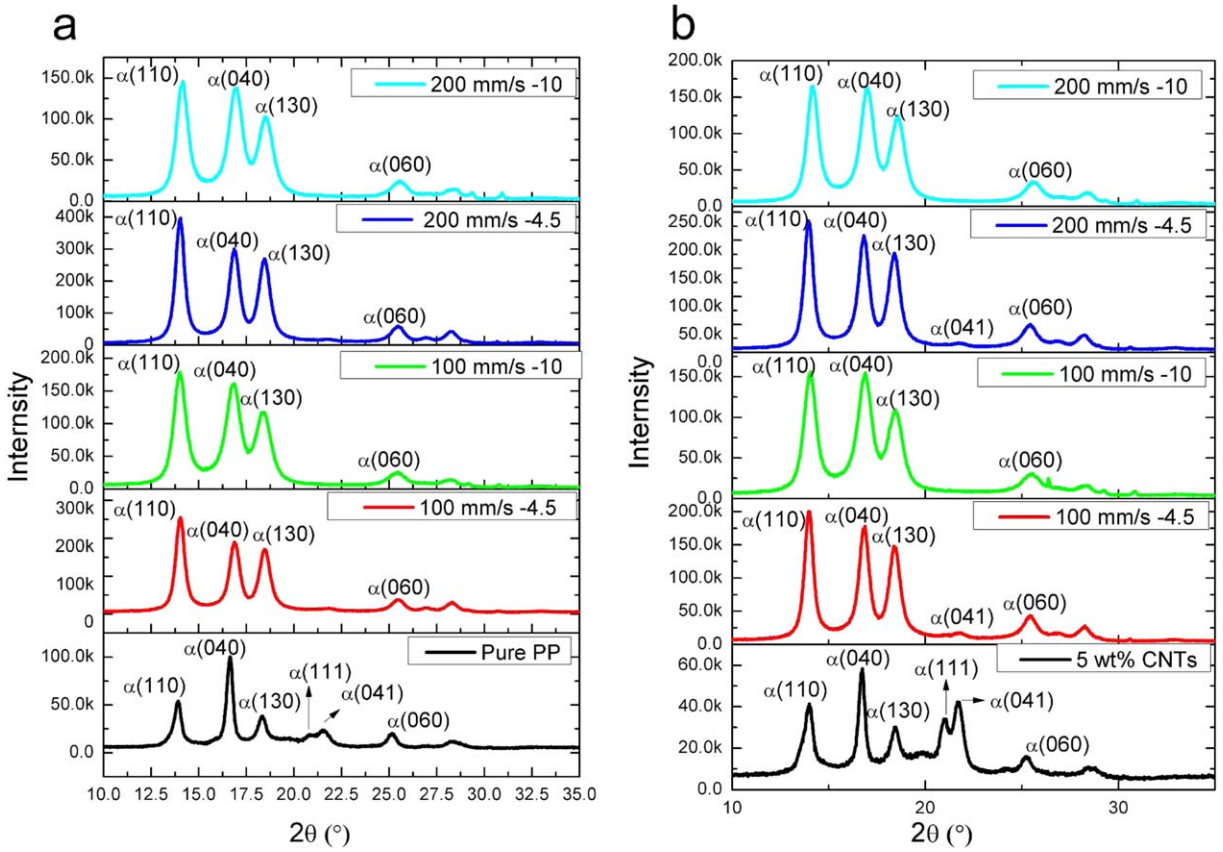

Figure 7. XRD patterns of the (a) pure PP and (b) PP/MWCNTs (5 wt %). [Color figure can be viewed in the online issue, which is available at wileyonlinelibrary.com.]

orientation and movement of the rearranged molecular chains were largely maintained after cooling. The effects of the MWCNT concentration, ν, and λ on the microstructure were considered through DSC measurements, as shown in Figure 6. The tested samples were named with the following convention: MWCNT content–ν–λ.

The fact that the intrinsic thermal properties of the PP matrix were hardly affected by the introduction of MWCNTs was revealed, but we still found that T_m decreased slightly with increasing MWCNT contents [Figure 6(a)], that is, from about 160.2°C (neat, 0%) to 158.2°C (5 wt %). After die drawing, a slight increase in T_m was revealed, even for the samples without MWCNT addition. We noticed that, however, for the billets stretched at high λ, a melting plateau including two or more T_ms were obtained in the DSC patterns, as shown in Figure 6(b,c). The melting region was expanded; this was attributed to the breakage of the crystal perfection, which caused the single T_m to change into a wide melting region. The conformational restrictions in the amorphous phase were broken down, and then secondary crystallization occurred. The expansion of T_m increased the melting enthalpy, which is generally used to calculate the crystallinity by the division of the ideal enthalpy of a 100% crystalline PP.

In addition, a higher λ was found to be more helpful for increasing the second T_m; this was also implied in the DSC measurements. As discussed previously, the original crystallites were broken down during die drawing, and new crystallites were reformed at the rubbery-state temperature. This was helpful for promoting the size growth of the crystallites. The XRD measurements were carried out to support this conjecture, as shown in Figure 7. The intensities of the dominant α phase at (110), (040), (130), and (060) increased simultaneously after drawing, but the intensities at (110) and (130) increased much more. The orientation behavior of the microstructure was further studied by WAXD measurements, as shown in Figure 8. We observed a significant orientation for the stretched samples, whereas it was hardly found for the unstretched sample. It made sense that the higher orientation degree was positively revealed from the samples with higher λs.

Dielectric Performance

The real and imaginary parts of the relative dielectric constant (ε' and ε'', respectively) could be calculated as follows:[32]

$$\varepsilon' = \frac{C_p d}{A\varepsilon_o} \tag{3}$$

$$\varepsilon'' = \frac{d}{A\omega\varepsilon_0 R_p} \tag{4}$$

$$\tan\delta = \frac{\varepsilon''}{\varepsilon'} \tag{5}$$

where C_p is the capacity, d is the specimen thickness, A is the area of the contact surface, ε_0 is the free-space permittivity, w is the frequency, and R_p is the equivalent parallel resistance.

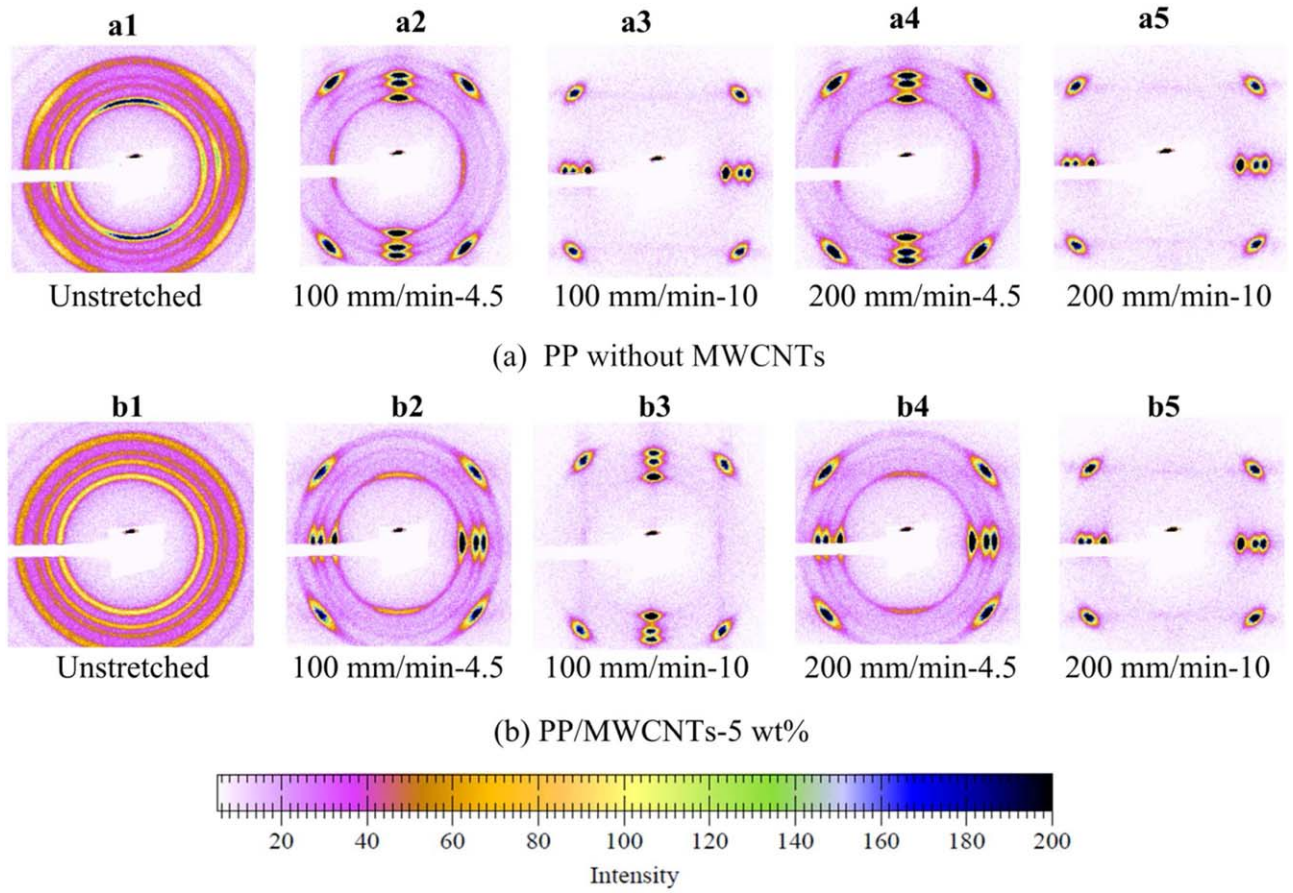

Figure 8. WAXD patterns of the (a) pure PP and (b) PP/MWCNTs (5 wt %). [Color figure can be viewed in the online issue, which is available at wileyonlinelibrary.com.]

Generally speaking, ε is related to ε'; that is, $\varepsilon' = \varepsilon$, which is a measure of how much energy can be stored in the material upon the application of an external electric field. Tan δ, representing the energy loss, includes Ohmic loss and polarization loss.

The increase ε in the polymer nanocomposites through the introduction of conductive particles was based on the enhancement of interfacial polarization.[3] As shown in Figure 9, both ε and tan δ increased with the loading of MWCNTs; this has also been revealed in other literature.[9,22] The introduction of the MWCNTs effectively increased ε, especially near the percolation threshold of the MWCNT concentration (between 2 and 5 wt %). Tan δ, however, also increased simultaneously; this caused a large energy consumption. However, the effects of v and λ could not be neglected.

With a high λ and a high v, both ε and tan δ decreased significantly. Tan δ of the stretched samples was as low as that of the neat PP when the loading of MWCNTs was no higher than 2 wt %; this is important for dielectric applications. Compared with pure PP, for example, ε of the samples with 2 wt % MWCNTs presented percentage increases of about 26.4% at $v = 100$ mm/s and $\lambda = 4.5$ and 29.2% of ε at $v = 200$ mm/s and $\lambda = 10$. The tan δ values of all of the tested samples with 2 wt % MWCNTs were almost the same, ranging from 0.005 to 0.01. As to the sample with 5 wt % MWCNTs, the ε values were 67.7 and 38.0 at $\lambda = 4.5$ and $vs = 100$ and 200 mm/s, respectively. When λ increased to 10, the ε values were 9.7 and 8.2 at $v = 100$ and 200 mm/s, decreasing by no more than one order of magnitude, respectively. The tan δ values, however, were 6.9 and 27.6 at $\lambda = 4.5$ and $v = 100$ and 200 mm/s and 0.68 and 0.25 at $\lambda = 10$ and $v = 100$ and 200 mm/s, respectively. A decrease in the order of magnitude of about 1–2 was revealed. This suggested that the high orientation of the microstructure not only decreased ε but also decreased tan δ more significantly. The fact that the decrease in tan δ was good for the exploration of practical applications of this PP/MWCNT nanocomposite is generally accepted.

The ε increase ratio (r), used to estimate the relationship between the orientation degree and dielectric performance, was defined by eq. (6) as follows:

$$r = \frac{\varepsilon_s}{\varepsilon_p} \tag{6}$$

where ε_s is the dielectric constant of a stretched sample at a certain frequency and ε_p is the dielectric constant of the pure PP (e.g., $\varepsilon_p = 2.38$ and tan $\delta = 0.01$ at 1 kHz). An overview of the enhancement of ε is given in Figure 10, in which r is calculated at a frequency of 1 kHz.

ε increased with increasing MWCNT content because of the enhancement of the electronic displacement polarization. A

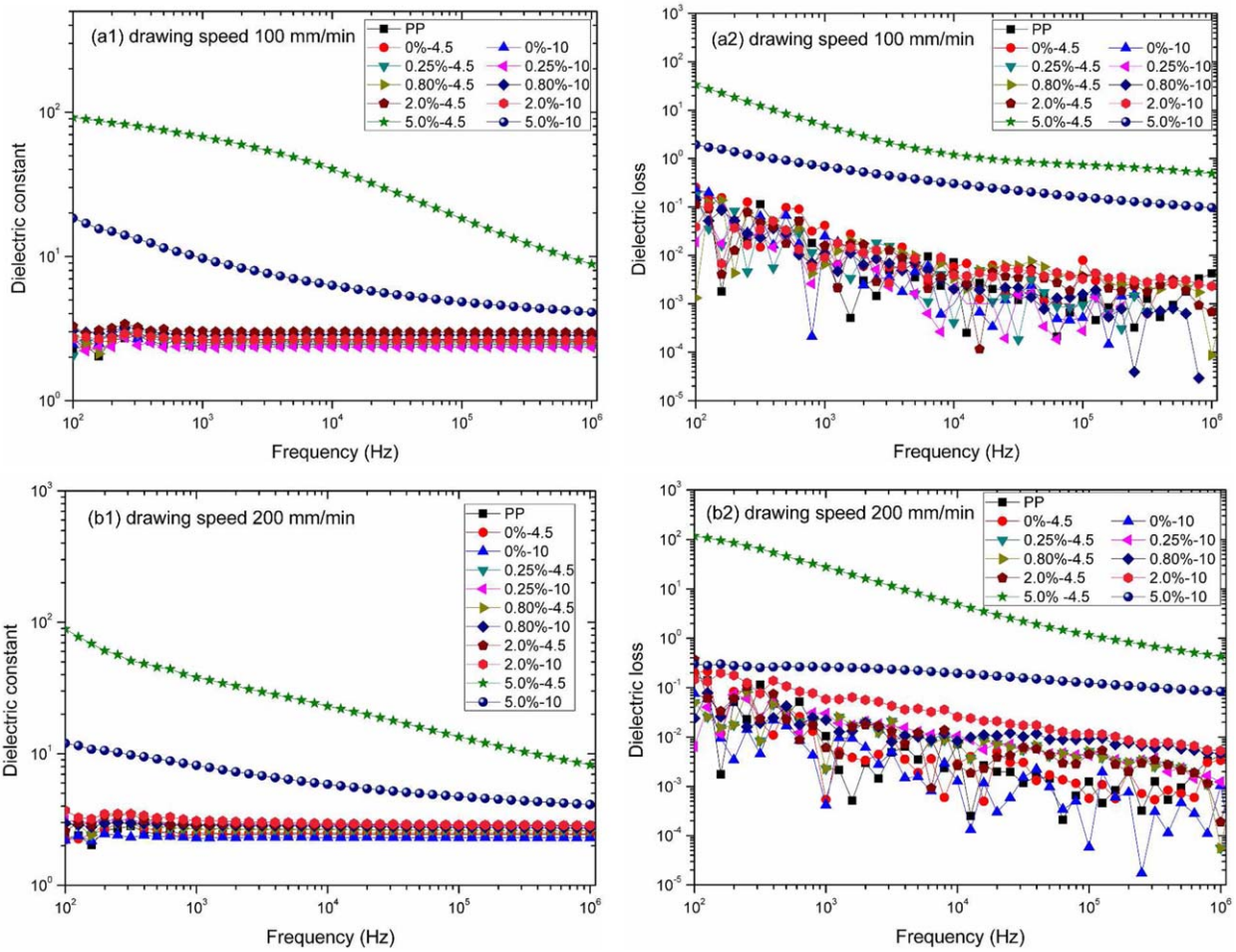

Figure 9. Dielectric performance of the PP or PP/MWCNTs drawn at (a) 100 and (b) 200 mm/s. [Color figure can be viewed in the online issue, which is available at wileyonlinelibrary.com.]

significant decrease in ε_s, however, was also found compared with ε_p. MWCNTs were dispersed within the PP matrix as individual tubes or aggregations in a random direction, and the construction of the conductive networks was obtained because of the clusters, as previously shown in Figure 2. The abrupt increase in ε_0 was attributed to this successful construction of the conductive networks, which were simultaneously introduced by plenty of free electrons. However, most of the networks were damaged during uniaxial drawing; this consequently decreased the electronic displacement polarization effect and then reduced ε. Meanwhile, the solid-phase orientation also confined the movement of molecular chains; this caused a decrease in the polarization effect of the dipole moment orientation. This conjecture was further confirmed by the resistivity measurement, as shown in Figure 11. The conductivity of the PP/MWCNT-5 wt % composites was taken as an example. In a comparison with the unstretched sample, the volume conductivity of drawn billets was obviously reduced by the die-drawing process. Although a higher orientation degree and more negative aggregated dispersion of MWCNTs were obtained at $\lambda = 10$, the volume resistivity of PP/MWCNT-5 wt % was lower than that at $\lambda = 4.5$. This was because the network connection between the MWCNTs was broken down along the drawing direction, but it could be bridged again along the d direction, as schematically shown in Figure 5(b). We still concluded that, therefore, the higher orientation degree of the microstructures of both

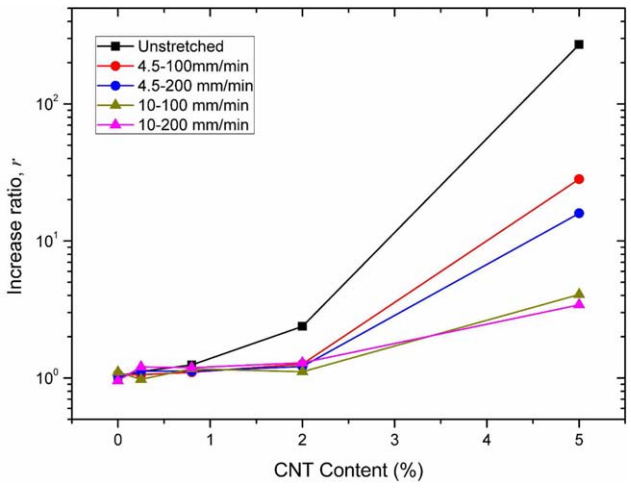

Figure 10. Dielectric constant ratios of the unstretched and stretched PP/MWCNTs at 1 kHz. [Color figure can be viewed in the online issue, which is available at wileyonlinelibrary.com.]

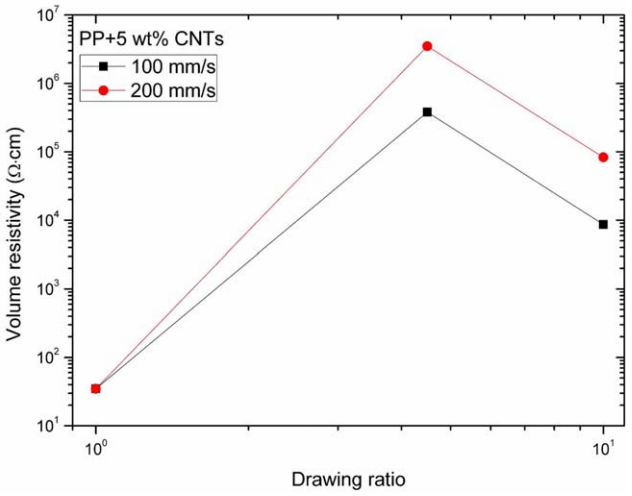

Figure 11. Volume resistivity of PP/MWCNT-5 wt % at different λs and *v*s. [Color figure can be viewed in the online issue, which is available at wileyonlinelibrary.com.]

MWCNT clusters and networks was, the lower ε_s were obtained. Well-dispersed MWCNTs remarkably improved the dielectric performance for the polymeric nanocomposites. A highly oriented solid phase not only changed the crystallization behavior of the polymer matrix, but it also changed the morphology of the MWCNT clusters or the dispersion state.

CONCLUSIONS

The dependence of the viscoelastic behavior and the dielectric dependence on the MWCNT concentration and the orientation effects of the microstructures were investigated in this study. A low MWCNT concentration was found to be helpful for decreasing the viscosity of the composite melt, increasing the flowability and viscous behavior because of the lubricant effect, and increasing the free volume. Solid-phase orientation was obtained through the die-drawing process performed at a rubbery-state temperature of about 140°C below the PP T_m. A wide melting plateau was clearly revealed from the DSC measurements; this indicated a damage of the crystal perfection and a second generation of new crystallite. The effect of the crystallization morphology transition on the dielectric properties was found to be negative in the enhancement of the polarization properties of the PP/MWCNTs; this led to a small-amplitude decrease of ε. It was suggested, however, that the aggregated MWCNT clusters or conductive networks were largely broken down by the highly uniaxial tensile strain; this remarkably decreased the electronic displacement polarization effect and then decreased ε and tan δ.

ACKNOWLEDGMENTS

The authors thank the National Natural Science Foundation of China (contract grant number NSFC51473018 and 51402015), the China Postdoctoral Science Foundation (contract grant number 2015M570928), and the Fundamental Research Funds for the Central Universities (contract grant number FRF-TP-14-013A1) for their financial support.

REFERENCES

1. Dang, Z. M.; Yuan, J. K.; Zha, J. W.; Zhou, T. Z.; Li, S. T.; Hu, G. H. *Prog. Mater. Sci.* **2012**, *57*, 660.
2. Selvi, M.; Vengatesan, M. R.; Prabunathan, P.; Song, J. K.; Alagar, M. *Appl. Phys. Lett.* **2013**, *103*, 152902.
3. Kim, J. Y.; Kim, T. Y.; Suk, J. W.; Chou, H.; Jang, J. H.; Lee, J. H.; Kholmanov, I. N.; Akinwande, D.; Ruoff, R. S. *Small* **2014**, *10*, 3405.
4. Arjmand, M.; Sundararaj, U. *Polym. Eng. Sci.* **2015**, *55*, 173.
5. Wang, Z.; Zhao, G. L. *J. Mater. Chem. C* **2014**, *2*, 9406.
6. da Silva, A. B.; Arjmand, M.; Sundararaj, U.; Bretas, R. E. S. *Polymer* **2014**, *55*, 226.
7. Sharma, M.; Madras, G.; Bose, S. *Phys. Chem. Chem. Phys.* **2014**, *16*, 2693.
8. Qiang, Z. X.; Liang, G. Z.; Gu, A. J.; Yuan, L. J. *Nanopart. Res.* **2014**, *16*, 2391.
9. Long, Y.; Pu, Z. J.; Huang, X.; Jia, K.; Liu, X. B. *J. Polym. Res.* **2014**, *21*, 525.
10. Guo, X. S.; Yu, D. M.; Wu, J. S.; Min, C.; Guo, R. N. *Polym. Eng. Sci.* **2013**, *53*, 370.
11. Zhang, W.; Ning, N. Y.; Gao, Y.; Xu, F.; Fu, Q. *Compos. Sci. Technol.* **2013**, *83*, 47.
12. Jouni, M.; Boiteus, G.; Massardier, V. *Polym. Adv. Technol.* **2013**, *24*, 909.
13. Xu, H.; Anlage, S. M.; Hu, L.; Gruner, G. *Appl. Phys. Lett.* **2007**, *90*, 183119.
14. Li, C.; Thostenson, E. T.; Chou, T. W. *Compos. Sci. Technol.* **2008**, *68*, 1227.
15. Zhang, S. H.; Zhang, N. Y.; Huang, C.; Ren, K. L.; Zhang, Q. M. *Adv. Mater.* **2005**, *17*, 1897.
16. Ameli, A.; Nofar, M.; Park, C. B.; Pötschke, P.; Rizvi, G. *Carbon* **2014**, *71*, 206.
17. de Luna, M. S.; Pellegrino, L.; Daghetta, M.; Mazzocchia, C. V.; Acierno, D.; Filippone, G. *Compos. Sci. Technol.* **2013**, *85*, 17.
18. Thomassin, J. M.; Trifkovic, M.; Alkarmo, W.; Detrembleur, C.; Jérôme, C.; Macosko, C. *Macromolecules* **2014**, *47*, 2149.
19. de Vivo, B.; Lamberti, P.; Spinelli, G.; Tucci, V. *J. Appl. Phys.* **2014**, *115*, 154311.
20. Zheng, P. L.; Pu, Z. J.; Yang, W.; Shen, S. Z.; Jia, K.; Liu, X. B. *J. Mater. Sci. Mater. Electron.* **2014**, *25*, 3833.
21. Baji, A.; Mai, Y. W.; Abtahi, M.; Wong, S. C.; Liu, Y.; Li, Q. *Compos. Sci. Technol.* **2013**, *88*, 1.
22. Tiberio, A. E.; José, C. C.; Alejandro, S.; Amelia, L. *Colloid Polym. Sci.* **2014**, *292*, 1989.
23. Fu, Y.; Liu, L. S.; Zhang, J. W. *ACS Appl. Mater. Interfaces* **2014**, *6*, 14069.
24. Dang, Z. M.; Yao, S. H.; Xu, H. P. *Appl. Phys. Lett.* **2007**, *90*, 012907.

25. Xu, W. H.; Ding, Y. C.; Jiang, S. H.; Zhu, J.; Ye, W.; Shen, Y. L.; Hou, H. Q. *Eur. Polym. J.* **2014**, *59*, 129.
26. Hou, H.; Ge, J. J.; Zeng, J.; Li, Q.; Reneker, D. H.; Greiner, A.; Cheng, S. Z. D. *Chem. Mater.* **2005**, *17*, 967.
27. Ning, N. Y.; Bai, X.; Yang, D.; Zhang, L. Q.; Lu, Y. L.; Nishi, T.; Tian, M. *RSC Adv.* **2014**, *4*, 4543.
28. Jain, S.; Goossens, J. P.; Peters, G. M.; van Duin, M.; Lamstra, P. *Soft Matter* **2008**, *4*, 1848.
29. Merkel, T. C.; Freeman, B. D.; Spontak, R. J.; He, Z.; Pinnau, I.; Meakin, P.; Hill, A. *Science* **2002**, *296*, 519.
30. Li, J.; Ma, P. C.; Chow, W. S.; To, C. K.; Tang, B. Z.; Kim, J. K. *Adv. Funct. Mater.* **2007**, *17*, 3207.
31. Coates, P. D.; Fin, C. R.; Ward, I. M.; Glen, T. *Sci. China Chem.* **2013**, *56*, 1017.
32. Osayuki, O.; Marianna, K.; Ribal, G. S.; Aristides, D. *Macromol. Mater. Eng.* **2015**, 300, 448.